Quasiperiodic oscillations for spherically symmetric regular black holes

Kuantay Boshkayev,[1,2,*] Anuar Idrissov,[3,4,†] Orlando Luongo,[1,5,6,7,‡] and Marco Muccino[1,§]

[1]*Al-Farabi Kazakh National University, Al-Farabi avenue 71, 050040 Almaty, Kazakhstan*
[2]*International Information Technology University, Manas street 34/1, 050040 Almaty, Kazakhstan*
[3]*Department of Physics, Nazarbayev University, Kabanbay Batyr 53, 010000 Astana, Kazakhstan*
[4]*Fesenkov Astrophysical Institute, Observatory 23, 050020 Almaty, Kazakhstan*
[5]*Università di Camerino, Via Madonna delle Carceri 9, 62032 Camerino, Italy*
[6]*SUNY Polytechnic Institute, 13502 Utica, New York, USA*
[7]*Istituto Nazionale di Fisica Nucleare, Sezione di Perugia, 06123, Perugia, Italy*

(Received 13 March 2023; accepted 2 August 2023; published 28 August 2023)

We consider the recent datasets of quasiperiodic oscillations from eight different low mass x-ray binaries. We here interpret their physical features in the context of given regular black hole solutions and verify their applicability to neutron stars. We evaluate the numerical constraints over the free parameters of Bardeen, Hayward, and Dymnikova regular solutions by performing a set of Markov chain Monte Carlo analyses, based on the Metropolis algorithm. For each source, we evaluate the best-fit parameters, among which the mass and the regularization scale or parameter, compare and contrast them with the current literature. We also infer the corresponding innermost stable circular orbit radii and the radial extents of the accretion disks. Focusing on how to identify discrepancies among theoretical models and observations, our results show that, in most of the cases, regular black holes, in particular the Bardeen and Hayward spacetimes are slightly more suitable to describe neutron stars than the Schwarzschild geometry, whereas the Dymnikova metric is ruled out.

DOI: 10.1103/PhysRevD.108.044063

I. INTRODUCTION

Recently, a novel interest in *black hole* (BH) physics arose due to the detection of *gravitational waves* first [1] and then to the impressive discovery of *BH shadows* [2], culminating to new confirmations of Einstein's general relativity[1] (GR). These findings determine a current understanding of BHs and may shed light on how, and whether, Einstein's gravity fails to be predictive. Consequently, all these advancements have led to the beginning of a new era based on *BH precision astronomy* [8].

In this fascinating scenario, low-mass x-ray binaries and microquasars may play a complementary role [9]. These sources exhibit narrow peaks of excess energy in their x-ray fluxes, named *quasiperiodic oscillations* (QPOs), that are associated with matter accretion into compact objects, providing information about the system and its overall properties. Analogously, they can be adopted to detect possible extensions of Einstein's gravity, becoming essential to furnish new data in the framework of BH astronomy. Such oscillations may conventionally be classified into two main typologies: *high-frequencies*, say 0.1–1 kHz, and *low frequencies*, say below 0.1 kHz [10,11]. Some models, for instance, suggest that the high frequencies are related to the Keplerian frequency close to the innermost stable circular orbit (ISCO) of test particles in accretion disks [12,13], whereas low frequencies are normally associated with periastron precession frequency [14–18].

Chronologically, QPOs were first discovered in white dwarfs [19–22] and later in the power spectra of x-ray binary NSs and BHs, leading to further studies of accretion disks [23–28]. QPOs provide a way to test gravity and to gather information about sources and cosmology [29]. Tight QPO frequency measurements obtained from accretion disks around compact objects help to determine the most suitable model for these astrophysical systems [30,31].

In the literature, there is a *plethora* of models describing QPOs data [32–41]. The most-accredited paradigm is the *relativistic precession model*, where QPOs emerge from the motion of inhomogeneities in accretion mechanism [42–46]. On the other hand, in the framework of alternative theories of gravity, it is also possible to describe QPOs involving GR approaches [47]. Finally, BH binaries may also exhibit

*kuantay@mail.ru
†anuar.idrissov@gmail.com
‡orlando.luongo@unicam.it
§muccino@lnf.infn.it

[1]For clarity, from the above breakthroughs we only argued tighter bounds on extended and/or modified theories of gravity [3–7]. However, no definitive conclusions are reached in regimes where gravity breaks down, i.e., quantum gravity epoch, strong field regimes, and so on.

QPOs, again classified into low and high frequencies [48–51]. Consequently, a definitive physical mechanism behind QPOs is not fully-understood yet, since their description can be intimately related to astrophysical BHs, whose theoretical features are currently under investigation [52,53].

In this puzzle, by virtue of Penrose and Hawking singularity theorems [54,55], the presence of matter satisfying reasonable energy conditions inevitably leads to singularities in GR. However, it is widely believed that such singularities can be healed introducing a complete theory of *quantum gravity*.

Thus, attempting to classically-overcome the above issue, Bardeen introduced the concept of a regular BH (RBH) [56], exhibiting no singularity at the center and asymptotic flatness, in a static spherical symmetry. Later, Ayón-Beato and García [57] demonstrated that the RHB *á la* Bardeen could be considered as a solution of Einstein's field equations coupled with a magnetic monopole source in the context of nonlinear electrodynamics [58]. Subsequently, other RBH models were proposed. For instance, Dymnikova [59] introduced a different type of RBH coinciding with the Schwarzschild spacetime at infinity and behaving as a de Sitter solution close to the center. Additionally, Hayward proposed a static and spherically symmetric RBH model to fulfill the BH information-loss paradox [60].

Recently, nonsingular BHs have gained an increasing interest. Below, we summarize some of their most recent applications to the gravitational collapse and astrophysical phenomena.

It has been introduced a class of static, nonsingular, asymptotically flat BHs encoding quantum corrections in a scale length smearing the singularity [61]. It has been showed that BHs with quantum effects at horizon scales, like a revisited RBH Hayward model with a quantum deformation parameter of the same order of the Schwarzschild radius, are thermodynamically preferred over those where the parameter is irrelevant. A particular case of RBH solutions belonging to the above non-singular class of models has been successfully able to model the orbit of the S2 star around the compact radio source Sagittarius A* (Sgr A*) in the center of our Galaxy [62].

Further, a novel rotating RBH metric [63] has been applied to model the x-ray NuSTAR spectrum of the Galactic BH in EXO 1846-031 and the data of the gravitational wave event GW190707A, with the aim of measuring the regularization parameter associated with this model [64]. The analysis provided limits on this parameter, being consistent with a vanishing value.

Finally, a comparison of shadow and ring properties of a Schwarzschild BH with those of Hayward BH, using the ray-tracing method on three optically thin accretion flow models, has been performed [65]. The results evidenced that the luminosities of both shadows and rings are influenced by properties of the accretion flows and the magnetic charge of the BH, whereas the BH singularity does not affect the generation of the shadow. The rotating generalization of Hayward's solution has been also applied to model Sgr A* [66]. The results showed that, even in the absence of a horizon, a resemblance to the shadow of a Kerr BH is obtained. To distinguish between the two geometries, QPO were suggested as possible mean to distinguish the two models on observational grounds [66].

Assuming that RBH solutions may also model neutron stars (NSs), we here investigate whether RBHs can be used in framing out sources of experimental QPO data, where the effects of (topological) charge cannot be excluded *a priori*. To do so, following recent studies, supporting the relativistic precession model, we hereafter associate QPO modes with the fundamental frequencies provided by a test-particle in the background metric, i.e., azimuthal (or Keplerian) frequency along with radial and vertical epicyclic frequencies. Thus, employing spherical symmetry, we work out the Bardeen, Hayward and Dymnikova spacetimes, and fit these metrics with the QPO data points. In so doing, we check whether it is plausible to use those configurations with the aim of describing the exterior of NSs. Specifically, the first two metrics assume the existence of a topological charge; only the third is constructed without this assumption.

Thus, in testing such solutions, we involve eight NS sources in the low mass x-ray binaries, considering their most updated QPO datasets. To test them, we numerically maximize the corresponding log-likelihoods, performing Markov chain Monte Carlo (MCMC) analyses, based on the *Metropolis-Hastings* algorithm, aiming to get best-fit parameters and the direct 1–σ and 2–σ error bars for each RBH solution. Guided by the NS interpretation and by the values of the ISCO of each metric, we show that in most cases RBHs are successful to model QPO frequencies and therefore conclude that the Schwarzschild metric does not represent the unique spacetime able to provide physical predictions from such sources. In particular, as by-product of our physical scrutiny, we see that the Bardeen and Hayward solutions appear favored, whereas the Dymnikova metric is *ruled out*. Physical consequences of our findings are also debated, comparing our outcomes with previous results, available in the literature.

The paper is organized as follows. In Sec. II, we describe QPO frequencies in the framework of the relativistic precession model. In Sec. III we introduce the proposed regular spacetimes, highlighting their physical main features. In Sec. IV, we perform MCMC analyses and, in Sec. V, we discuss the physical interpretations and their theoretical implications. In Sec. VI, we report conclusions and perspectives of the work.

Throughout this paper we use natural units, $G = c = \hbar = 1$, and Lorentzian signature $(-,+,+,+)$.

II. QUASIPERIODIC OSCILLATIONS

QPOs are not strictly periodic oscillations, prompting a slightly varying set of frequencies that can be viewed as nearly constant. These frequencies are often observed in astrophysical systems, among which accretion disks around BHs, NSs and, in a broad sense, from strong gravity compact objects.

The harmonic oscillation we refer to is related to the fundamental or epicyclic frequencies of test particles moving in circular orbits within accretion disks around compact objects. To estimate such frequencies, we start with a test particle Lagrangian

$$\mathbb{L} = \frac{1}{2} m g_{\mu\nu} \dot{x}^\mu \dot{x}^\nu, \tag{1}$$

where m is the test particle mass and x^μ are four-coordinates with $\mu = 0, 1, 2, 3$. Here, $\dot{x}^\mu = dx^\mu/d\tau$ represent their four-velocities. Since we have static metrics, the killing vectors imply conserved quantities, say the specific energy, $\mathcal{E} = -g_{tt}\dot{t}$, and the angular momentum, $\mathcal{L} = g_{\phi\phi}\dot{\phi}$. From the four-velocity normalization condition $g_{\mu\nu}\dot{x}^\mu\dot{x}^\nu = -1$ of massive test particles, one gets the four-velocity radial component.

Thus, as $m \neq 0$, the integrals of motion read

$$\dot{t} = -\frac{\mathcal{E}}{g_{tt}}, \qquad \dot{\phi} = \frac{\mathcal{L}}{g_{\phi\phi}}, \qquad g_{rr}\dot{r}^2 + g_{\theta\theta}\dot{\theta}^2 = V_{\text{eff}}, \tag{2}$$

where the effective potential, V_{eff}, is defined as

$$V_{\text{eff}} = -1 - \frac{\mathcal{E}^2 g_{\phi\phi} + \mathcal{L}^2 g_{tt}}{g_{tt} g_{\phi\phi}}. \tag{3}$$

For circular orbits on the equatorial plane, the conditions $\dot{r} = \dot{\theta} = 0$ lead to the test particle orbital equations

$$\Omega_\phi = \pm\sqrt{-\frac{\partial_r g_{tt}}{\partial_r g_{\phi\phi}}}, \tag{4a}$$

$$\dot{t} = u^t = \frac{1}{\sqrt{-g_{tt} - g_{\phi\phi}\Omega_\phi^2}}, \tag{4b}$$

$$\mathcal{E} = -\frac{g_{tt}}{\sqrt{-g_{tt} - g_{\phi\phi}\Omega_\phi^2}}, \tag{4c}$$

$$\mathcal{L} = \frac{g_{tt}\Omega_\phi}{\sqrt{-g_{tt} - g_{\phi\phi}\Omega_\phi^2}}, \tag{4d}$$

where the signs "±" in Eq. (4a) refer to clockwise and counter clockwise orbits, respectively [67].

A. The ansatz of small oscillations

In the small oscillations regime, the displacements from equilibrium positions, $r \sim r_0 + \delta r$ and $\theta \sim \pi/2 + \delta\theta$, imply

$$\frac{d^2\delta r}{dt} + \Omega_r^2 \delta r = 0, \qquad \frac{d^2\delta\theta}{dt} + \Omega_\theta^2 \delta\theta = 0, \tag{5}$$

with corresponding frequencies

$$\Omega_r^2 = -\frac{1}{2g_{rr}(u^t)^2}\partial_r^2 V_{\text{eff}}(r,\theta)\Big|_{\theta=\pi/2}, \tag{6a}$$

$$\Omega_\theta^2 = -\frac{1}{2g_{\theta\theta}(u^t)^2}\partial_\theta^2 V_{\text{eff}}(r,\theta)\Big|_{\theta=\pi/2}, \tag{6b}$$

for radial and angular coordinates, respectively. From the above angular frequencies, we define the Keplerian frequency $f_\phi = \Omega_\phi/(2\pi)$ and the radial epicyclic frequency of the Keplerian motion $f_r = \Omega_r/(2\pi)$. The relativistic precession model identifies the lower QPO frequency f_L with the periastron precession, namely $f_L = f_\phi - f_r$, and the upper QPO frequency f_U with the Keplerian frequency, namely $f_U = f_\phi$ [68,69].

III. STATIC SPHERICALLY SYMMETRIC REGULAR BLACK HOLES

The simplest approach that permits to describe compact object involves the use of a spherically symmetric, nonrotating metric. In particular, the spacetime geometry can be characterized through

$$ds^2 = -f(r)dt^2 + f(r)^{-1}dr^2 + r^2(d\theta^2 + \sin^2\theta d\phi^2), \tag{7}$$

also involving the class of metrics that exhibit electrically charged object in GR, see e.g., [70] and furthermore being adaptable to find out solution in extended theories of gravity. Hereafter, we focus on the above class of metric employing regular configurations represented by three RBH solutions: the Bardeen, Hayward, and Dymnikova spacetimes. The reason behind the choice of such metrics is that their structures appear particularly simple and apparently well-adaptable to the cases of our interest from which we argue our QPO data points. Below, we elucidate the main features of each spacetime, emphasizing the physical properties that will be discussed in comparing our numerical findings.

A. Bardeen metric

The Bardeen metric [56,57] is a solution of Einstein's field equations that represents a nonrotating BH with topological charge, whose lapse function was first derived by John Bardeen in 1968, with the underlying motivation to find a solution to Einstein-Maxwell equations describing a

magnetically-charged BH, as an alternative to the traditional Reissner-Nordström BH solution.

Consequently, the lapse function can be written as

$$f(r) = 1 - \frac{2Mr^2}{(r^2+q^2)^{3/2}}, \tag{8}$$

where M is the mass and q is the parameter responsible for the smearing of the singularity that plays the role of the magnetic charge. For vanishing q the Bardeen metric reduces to the Schwarzschild BH, whereas its rotating version, like many rotating RBHs obtained through the Newman-Janis (NJ) algorithm [71], reduces to the Kerr solution at large distances or for vanishing q.

The NJ algorithm is widely used in the literature to construct rotating solutions to the Einstein field equations from the known static, spherically symmetric, seed black hole and worm hole solutions [72–78]. Despite being successful in generating new solutions with rotation, this algorithm has some limitations. For example, according to Ref. [79] the application of this algorithm to an arbitrary non-GR spherically symmetric solution introduces pathologies in the resulting axially symmetric metric. In Ref. [80] it has been shown that new stationary generalizations of static vacuum solutions, in terms of the NJ algorithm, do not preserve the conformal symmetry. In addition, the application of this algorithm to static solutions with axial symmetry is an open issue.

Thus, adopting the strategy presented in Eqs. (6), one can write the fundamental frequencies for test particles

$$\Omega_\phi^2 = \frac{M(r^2-2q^2)}{(r^2+q^2)^{5/2}}, \tag{9a}$$

$$\Omega_\theta^2 = \Omega_\phi^2, \tag{9b}$$

$$\Omega_r^2 = \frac{M(r^6+9q^2r^4-8q^6)}{(r^2+q^2)^{9/2}} - \frac{6M^2r^6}{(r^2+q^2)^5}, \tag{9c}$$

where Ω_ϕ represents the Keplerian angular velocity of a test particle measured by an observer placed at infinity, Ω_r is the radial angular velocity and Ω_θ is the vertical angular velocity. Last but not least, it is remarkable to stress that the physical interpretation of q is provided by the existence of monopole charge of the self-gravitating magnetic field. Thus, the Bardeen metric, if applied to exteriors of compact objects, will provide information about the net charge associated with them, in terms of a monopole nonlinear charge. We will check later the goodness of this hypothesis in the framework of QPOs.

B. Hayward metric

First suggested by Poisson and Israel in 1988 [81], later in 2006 Hayward [60] rederived a regular BH spacetime that resembles the physical interpretation of the Bardeen one. This RBH implies a specific matter energy-momentum tensor that is de Sitter at the core and vanishes at large distances $r \to \infty$ [60]. The lapse function $f(r)$ for the Hayward BH takes a simple form

$$f(r) = 1 - \frac{2Mr^2}{r^3+q^3}, \tag{10}$$

where M is the mass of the BH, r is the radial coordinate, and q is the smearing length scale. In Ref. [60], the smearing parameter is given by $q = (2a^2)^{1/3}$, where $a^2 = 3M/\Lambda$ and Λ is the de Sitter cosmological constant. Therefore, in the following, we choose (M, a) as the fitting parameters.

Again, from Eqs. (6) the fundamental frequencies read

$$\Omega_\phi^2 = \frac{M(r^3-2q^3)}{(r^3+q^3)^2}, \tag{11a}$$

$$\Omega_\theta^2 = \Omega_\phi^2, \tag{11b}$$

$$\Omega_r^2 = \frac{M[r^5(r-6M)+11q^3r^3-8q^6]}{(r^3+q^3)^3}. \tag{11c}$$

For the sake of completeness, it is remarkable to notice that both Bardeen and Hayward metrics can be inspired by the Damour–Solodukhin scenario where a line element, with distinct lapse and shift functions, was introduced to provide a class of solutions including Bardeen and Hayward [82].

C. Dymnikova metric

The Dymnikova metric is based on the idea that the gravitational field of a BH can be described by a non-symmetric metric, which takes into account the presence of a nonzero energy-momentum tensor in proximity of the BH [83]. This approach allows for a more accurate description of the gravitational field of a BH and its effects on the surrounding space-time. The lapse function for Dymnikova's solution is of the following form

$$f(r) = 1 - \frac{2M}{r}\frac{2}{\pi}\left[\arctan\left(\frac{r}{q}\right) - \frac{rq}{r^2+q^2}\right], \tag{12}$$

where $q = \pi w^2/(8M)$ is the length scale, M is the total mass, and w is the charge. In the following, we choose (M, w) as the fitting parameters.

Within the Dymnikova metric, the fundamental angular frequencies are

$$\Omega_\phi^2 = \frac{2M}{\pi r^3}\left[\arctan\left(\frac{r}{q}\right) - \frac{rq(3r^2+q^2)}{(r^2+q^2)^2}\right], \tag{13a}$$

$$\Omega_\theta^2 = \Omega_\phi^2, \tag{13b}$$

$$\Omega_r^2 = \frac{2M}{\pi^2 r^4 (r^2+q^2)^3}\left\{ r^2 q[-4Mq(17r^2+3q^2)+\pi(r^4-8r^2q^2-q^4)] + \arctan\left(\frac{r}{q}\right)\left[-12M(r^2+q^2)^3 \arctan\left(\frac{r}{q}\right) + 8Mrq(6r^4+13r^2q^2+3q^4)+\pi r(r^2+q^2)^3\right]\right\}. \quad (13c)$$

IV. NUMERICAL ANALYSIS

In order to numerically check our theoretical frameworks with data, we modify the free-available *Wolfram Mathematica* code developed in Ref. [84] to work out our MCMC analyses, based on the Metropolis-Hastings algorithm. We thus find the best-fit parameters resulting from the maximum of the log-likelihood, defined by

$$\ln L = -\sum_{k=1}^{N}\left\{\frac{[f_{\rm L}^k - f_{\rm L}(p,\overline{f_{\rm U}^k})]^2}{2(\sigma_{\rm L}^k)^2} + \ln(\sqrt{2\pi}\sigma_{\rm L}^k)\right\}, \quad (14)$$

where p labels the model parameters and N the data for each source, sampled as lower frequencies $f_{\rm L}^k$, attached errors $\sigma_{\rm L}^k$, and *error-averaged* upper frequencies $\overline{f_{\rm U}^k}$, which will be better explained below. Not all the metrics considered in this work have analytic expressions for $f_{\rm L} = f_{\rm L}(p, f_{\rm U})$. Therefore, to run our MCMC simulations, we followed the steps described below.

(I) For each data point f_U^k and each metric, we invert the equations $f_U^k = f_U^k(p, r^k)$ numerically and we find the radial coordinate solutions $r^k \equiv r^k(p, f_{\rm U}^k)$.

(II) To account for the errors $\sigma_{\rm U}^k$, we find the solutions $r_+^k \equiv r_+^k(p, f_{\rm U}^k + \sigma_{\rm U}^k)$ and $r_-^k \equiv r_-^k(p, f_{\rm U}^k - \sigma_{\rm U}^k)$, where "+" and "−" indicate the solutions of r obtained from $f_{\rm U}^k + \sigma_{\rm U}^k$ and $f_{\rm U}^k - \sigma_{\rm U}^k$, respectively.

(III) We compute *error-averaged* solutions $\overline{r^k} = (r_+^k + r_-^k)/2$, which essentially are functions of what can be defined as *error-averaged* upper frequencies $\overline{f_{\rm U}^k}$.

(IV) Finally, we compute the theoretical lower frequencies $f_{\rm L} = f_{\rm L}[p, \overline{r^k}(p, \overline{f_{\rm U}^k})] \equiv f_{\rm L}(p, \overline{f_{\rm U}^k})$, which implicitly include also the uncertainties $\sigma_{\rm U}^k$.

Following the above procedure, we performed the fits of the $f_{\rm L}$–$f_{\rm U}$ frequencies of each source by using the four models here adopted. Fig. 1 showcases the corresponding $f_{\rm L}$–$f_{\rm U}$ best-fit curves, while Figs. 3–5 of the Appendix display the contour plots of the model parameters. The contours show the goodness of our findings up to 2–σ. As it appears evident, not all the fits smoothly converge as likely due to the lack of large data point number. The corresponding σ values are then affected by large error bars. This will reflect consequences on our theoretical conclusions, as discussed below.

The results of the fits are summarized in Tables I and II. In particular, the best-fit results of Table I are listed in terms of the RBH mass M and the smearing of the singularity q (see Secs. III A–III C for the relations between q and the model parameters of each regular solution). The motivation of this choice is that, from an observational point of view, the smearing parameters q of all the regular solution represent purely phenomenological parameters, although derived as solutions of different theories with different physical meanings.

V. THEORETICAL DISCUSSION

In this section, we argue some physical consequences based on the information summarized in Tables I–II. There, for each source, we can establish the best-fit model out of the four metrics considered throughout this work.

To compare each fit, based on different metric, we employ the well-consolidated *Aikake information criterion* (AIC) and *Bayesian information criterion* (BIC) [85]. They read

$$\mathrm{AIC} = -2\ln L + 2p, \quad (15a)$$

$$\mathrm{BIC} = -2\ln L + p\ln N, \quad (15b)$$

where the maximum value of the log-likelihood $\ln L$ is taken from our findings reported in Table I.

If we label with AIC_0 and BIC_0 the lowest values of the AIC and BIC tests, the model with these values is referred to as the fiducial (best-suited) model and the other models compare with the fiducial one via the difference $\Delta\mathrm{AIC}/\Delta\mathrm{BIC} = \mathrm{AIC/BIC} - \mathrm{AIC}_0/\mathrm{BIC}_0$. These differences provide evidence against the proposed model or, equivalently, in favor of the fiducial one, as follows

(i) ΔAIC or ΔBIC $\in [0,3]$, weak evidence;
(ii) ΔAIC or ΔBIC $\in (3,6]$, mild evidence;
(iii) ΔAIC or ΔBIC > 6, strong evidence.

For each QPO source, we discuss the results from statistical, observational and physical points of view. In what follows, we want to stress that, though depending on the equation-of-state, theoretically one can have larger masses up $6.1M_\odot$, albeit from observations we now get up to $2.14M_\odot$ [86]. We will *disentangle* this concept in our theoretical interpretations below.

(i) Cir X-1 [87]. From Table I, we notice that Bardeen and Dymnikova metrics are equally, strongly preferred over the other ones and, from Table II, these RBH solutions provide suitable physical values for the ISCO. However, in both cases we obtain masses $M \gtrsim 3M_\odot$, which seems incompatible with the NS interpretation supported by Ref. [88]. However, if

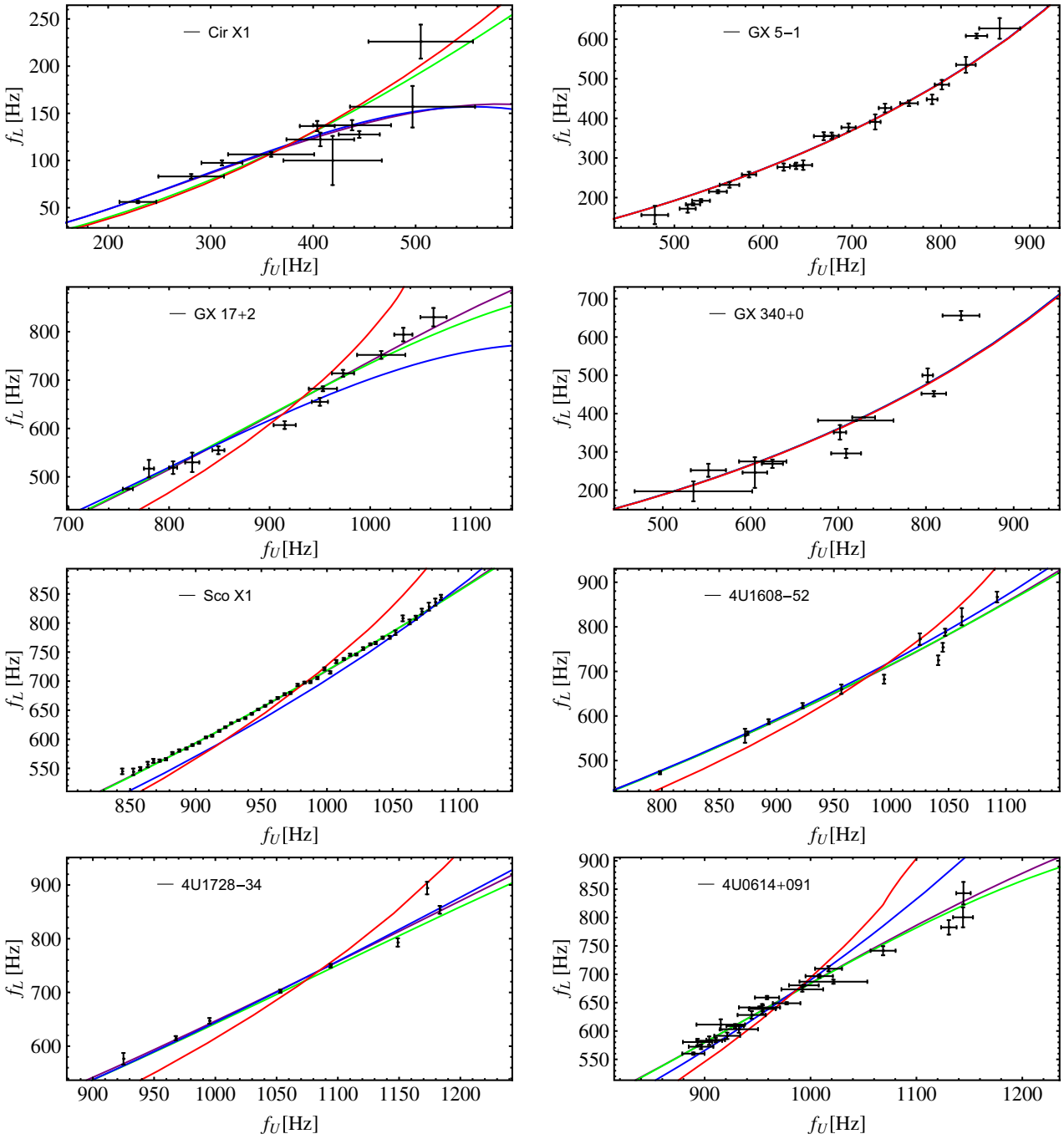

FIG. 1. Plots of $f_{\rm L}$ vs $f_{\rm U}$ frequencies of the QPO datasets considered in this work (black data with error bars). Fits have been performed by using Schwarzschild (red), Hayward (green), Bardeen (purple) and Dymnikova (blue) spacetimes.

we consider the absolute upper limit of $M_{\rm up} = 6.1 M_\odot$, Bardeen RBH provides a mass below $M_{\rm up}$, whereas Dymnikova RBH does not. Therefore, we conclude that Bardeen RBH is the favored solution from the statistical, theoretical and experimental perspectives.

(ii) GX 5-1 [89,90], GX $17+2$ [91], GX $340+0$ [92]. Looking at Tables I–II for the source GX 5-1, we notice that all models do provide good fits to the data and physical values for the ISCO. From a statistical viewpoint, the Schwarzschild metric with its parameters represents the fiducial model that provides a well constrained mass, compatible with current NS mass observations. Hence, we conclude that it represents the best-fit model. Similar conclusions, but with stronger evidences against the more complicated models, can be reached also for the source GX $340+0$, where all the RBHs are statistically

TABLE I. Best-fit parameters with the associated $1-\sigma$ error bars obtained from Hayward (H), Bardeen (B) and Dymnikova (D) metrics. ΔAIC and ΔBIC are computed with respect to the reference model, i.e., the model with the highest value of $\ln L$. For comparisons, we also reported the results from the Schwarzschild (S) metric obtained in Ref. [47].

Source	Metric	M ($M_\odot$)	q (km)	q/M	**Horizon**	$\ln L$	AIC	BIC	ΔAIC	ΔBIC
Cir X1	S	$2.224^{+0.029}_{-0.029}$	⋯	⋯	⋯	−125.84	254	254	145	145
	H	$2.466^{+0.061}_{-0.038}$	$5.820^{+0.028}_{-0.239}$	1.605	No	−105.77	216	216	107	107
	B	$4.74^{+0.23}_{-0.23}$	$9.34^{+0.47}_{-0.52}$	1.340	No	−52.23	109	109	0	0
	D	$7.491^{+0.067}_{-0.845}$	$7.79^{+0.12}_{-1.57}$	0.707	No	−52.33	109	109	0	0
GX 5–1	S	$2.161^{+0.010}_{-0.010}$	⋯	⋯	⋯	−200.33	403	404	0	0
	H	$2.163^{+0.015}_{-0.017}$	$0.56^{+0.79}_{-0.56}$	0.176	Yes	−200.32	405	407	2	3
	B	$2.164^{+0.017}_{-0.020}$	$0.14^{+0.28}_{-0.14}$	0.044	Yes	−200.34	405	407	2	3
	D	$2.177^{+0.046}_{-0.032}$	$0.027^{+0.061}_{-0.027}$	0.008	Yes	−200.44	405	407	2	3
GX 17 + 2	S	$2.07678^{+0.0002}_{-0.0003}$	⋯	⋯	⋯	−1819.02	3640	3641	3513	3513
	H	$3.111^{+0.023}_{-0.022}$	$6.894^{+0.057}_{-0.079}$	1.507	No	−61.67	127	128	0	0
	B	$3.803^{+0.008}_{-0.020}$	$5.488^{+0.009}_{-0.043}$	0.981	No	−61.81	128	129	1	1
	D	$5.8124^{+0.0064}_{-0.0073}$	$4.762^{+0.011}_{-0.010}$	0.557	No	−217.15	438	439	311	311
GX 340 + 0	S	$2.102^{+0.003}_{-0.003}$	⋯	⋯	⋯	−130.86	264	264	0	0
	H	$2.112^{+0.013}_{-0.008}$	$0.90^{+1.02}_{-0.90}$	0.289	Yes	−134.17	273	273	9	9
	B	$2.113^{+0.025}_{-0.010}$	$0.28^{+0.42}_{-0.28}$	0.090	Yes	−134.13	273	273	9	9
	D	$2.137^{+0.081}_{-0.036}$	$0.058^{+0.113}_{-0.058}$	0.018	Yes	−134.10	273	273	9	9
Sco X1	S	$1.9649^{+0.0005}_{-0.0005}$	⋯	⋯	⋯	−3887.17	7776	7779	7503	7503
	H	$2.659^{+0.014}_{-0.006}$	$5.680^{+0.046}_{-0.020}$	1.453	No	−137.03	278	281	5	5
	B	$3.242^{+0.017}_{-0.015}$	$4.536^{+0.035}_{-0.029}$	0.952	No	−134.56	273	276	0	0
	D	$3.831^{+0.044}_{-0.711}$	$2.827^{+0.037}_{-1.145}$	0.502	No	−2591.17	5187	5190	4914	4914
4U1608–52	S	$1.960^{+0.004}_{-0.004}$	⋯	⋯	⋯	−235.83	474	475	348	348
	H	$2.627^{+0.044}_{-0.039}$	$5.59^{+0.15}_{-0.13}$	1.447	No	−60.96	127	128	1	1
	B	$3.180^{+0.061}_{-0.064}$	$4.43^{+0.12}_{-0.13}$	0.947	No	−60.85	126	127	0	0
	D	$4.373^{+0.016}_{-0.125}$	$3.384^{+0.030}_{-0.190}$	0.526	No	−65.35	135	136	9	9
4U1728–34	S	$1.734^{+0.003}_{-0.003}$	⋯	⋯	⋯	−212.61	427	427	349	349
	H	$2.470^{+0.034}_{-0.046}$	$5.44^{+0.10}_{-0.14}$	1.498	No	−45.17	94	94	15	15
	B	$3.055^{+0.062}_{-0.064}$	$4.41^{+0.11}_{-0.12}$	0.982	No	−37.27	79	79	0	0
	D	$4.170^{+0.021}_{-0.014}$	$3.334^{+0.033}_{-0.023}$	0.544	No	−38.47	81	81	2	2
4U0614 + 091	S	$1.904^{+0.001}_{-0.001}$	⋯	⋯	⋯	−842.97	1688	1691	1398	1398
	H	$2.808^{+0.028}_{-0.022}$	$6.274^{+0.079}_{-0.064}$	1.520	No	−143.09	290	293	0	0
	B	$3.509^{+0.011}_{-0.032}$	$5.126^{+0.023}_{-0.054}$	0.993	No	−146.22	296	299	6	6
	D	$4.0282^{+0.0041}_{-0.0079}$	$3.0775^{+0.0061}_{-0.0131}$	0.520	No	−266.85	538	541	248	248

disfavored. On the contrary, in the case of GX 17 + 2, Hayward and Bardeen metrics equally best-fit the data (see Table I). The Hayward metric provides a mass which is barely consistent with the NS interpretation, if one considers extremely rotating NSs with stiff equations-of-state [93], while the mass inferred from the Bardeen metric is not consistent at all with any NS observations, albeit theoretically not fully excluded. On the ground of these considerations, the Hayward and Bardeen metrics provide the best-fitting and physically allowed solutions that correctly describe GX 17 + 2.

(iii) Sco X1 [94]. From Table I, the best fit is given by the Bardeen metric, mildly preferred over the Hayward one. Even in this case, the main caveat is related to the mass: Bardeen metric provides a mass which is barely consistent with that of a very extreme NS [93], while the mass $\approx 2.7 M_\odot$ obtained from the Hayward metric is in the acceptable observational range [95]. Moreover, from Table II all the RBH metrics do provide physical ISCO values. Therefore, the Bardeen and Hayward metrics do give the only physical fit for this source. It is worth mentioning that the masses inferred from the Bardeen and

TABLE II. Numerical values of ISCO and inner and outer disk radii for each source have been computed from best-fit results of Table I. Thus, according to the ISCO values one cannot exclude/rule out RBH solutions.

Source	Model	ISCO (km)	Inner (km)	Outer (km)
Cir X1	S	19.62	30.79	52.16
	H	5.74	31.60	53.90
	B	9.76	35.70	65.08
	D	10.44	36.24	70.13
GX $5-1$	S	19.06	21.29	31.63
	H	19.07	21.29	31.64
	B	19.08	21.29	31.65
	D	19.10	21.31	31.69
GX $17+2$	S	18.32	18.33	22.94
	H	6.88	19.80	25.56
	B	6.12	19.98	26.27
	D	6.80	19.33	26.71
GX $340+0$	S	18.54	21.52	29.07
	H	18.61	21.55	29.12
	B	18.60	21.55	29.12
	D	18.62	21.59	29.19
Sco X1	S	17.33	17.72	20.98
	H	5.72	18.90	22.72
	B	16.02	19.25	23.42
	D	17.08	19.00	23.22
4U1608-52	S	17.29	17.65	21.75
	H	5.64	18.78	23.56
	B	16.22	19.12	24.31
	D	16.58	19.08	24.74
4U1728-34	S	15.29	16.06	18.93
	H	5.44	17.33	20.79
	B	4.92	17.64	21.45
	D	4.81	17.49	21.62
4U0614 + 091	S	16.80	16.95	20.05
	H	6.26	18.26	22.13
	B	5.70	18.47	22.76
	D	16.26	18.19	22.39

Hayward metrics (see Table I) are inconsistent with the range 1.40–1.52$M_\odot$, obtained by modeling optical light curves of Sco X1 [96]. This fact suggests that all the considered metrics do not accurately describe the QPO data of Sco X1, therefore, further analyses will be performed in future works.

(iv) 4U1608-52 [97], 4U1728-34 [98], 4U0614 + 091 [99]. The considerations reached for 4U1608-52 are analogous to the previous case of Sco X1, with the best fit given by the Bardeen metric slightly preferred over the Hayward one. Again, the Hayward metrics provide a mass which is not as extreme as for the Bardeen metric, all of them theoretically not fully-excluded. For 4U1728-34, the Bardeen and Dymnikova metrics perform equally well, but Bardeen metric does provide an extreme NS mass, still consistent with the upper limit from Ref. [96], whereas Dymnikova does not, albeit still below $M_{\rm up}$. For 4U0614 + 091, the best fit model is obtained unambiguously from the Hayward metric because it is the fiducial model and from a physical point of view provides both a NS-like mass and a physical values of the ISCO.

Using the best-fit values of Table I, we are now in the position to understand which RBH configuration (two-horizon, extremal or horizon-less) is preferred by the data. The horizon of a RBH is defined in analogy with a singular BH by imposing $1/g_{rr}=0$ condition. For the considered spherically solution the condition is equivalent to $f(r)=0$, which yields several roots, among which only two describe the inner and outer horizons and the other ones are nonphysical. Bardeen and Hayward RBHs have horizon radii with analytic expressions, whereas for Dymnikova RBH these can be computed only numerically, due to the transcendent form of the equation.

In Fig. 2 we show the radii of inner and outer horizons normalized by the mass, r_H/M, versus the smearing parameters normalized by the mass, q/M, for Bardeen (top panel), Hayward (middle panel), and Dymnikova RBHs (bottom panel). For all solutions, the dashed black line indicates the boundary between inner and outer horizons. The values of r_H/M and q/M at the border correspond to the extreme BH cases. For vanishing q/M the inner horizon r_H/M tends to 0, whereas the outer horizon tends to 2 in all models. As one may notice, the horizons can be present only for certain ranges of the ratio q/M, namely from 0 to $\approx$1.0583 for Hayward, to $\approx$0.7698 for Bardeen, and to $\approx$0.4522 for Dymnikova. There is no horizon beyond the indicated range. For more details see Table I, where the presence (or absence) of the horizons have been derived by assessing the ratio q/M inferred from the QPOs best-fits.

The results of Table I, indicate that most of the sources considered in this work can be successfully modeled by horizon-less configurations. Only two cases, i.e., GX 5–1 ad GX $340+0$, admit horizons. However, this is not surprising because for these sources the best-fit is provided by the Schwarzschild spacetime, which has a horizon by definition, and all the RBH fits provide values of the parameter q consistent with zero, in favor of the extremal configuration interpretation.

We thus can finally conclude that, guided by the NS physical interpretation of mass constraints and by the values obtained for the ISCOs, the Schwarzschild metric *is not the only physically allowed solution* and turns out to be disfavored for most of the above listed QPO sources. For all the sources, the Bardeen and Hayward solutions are

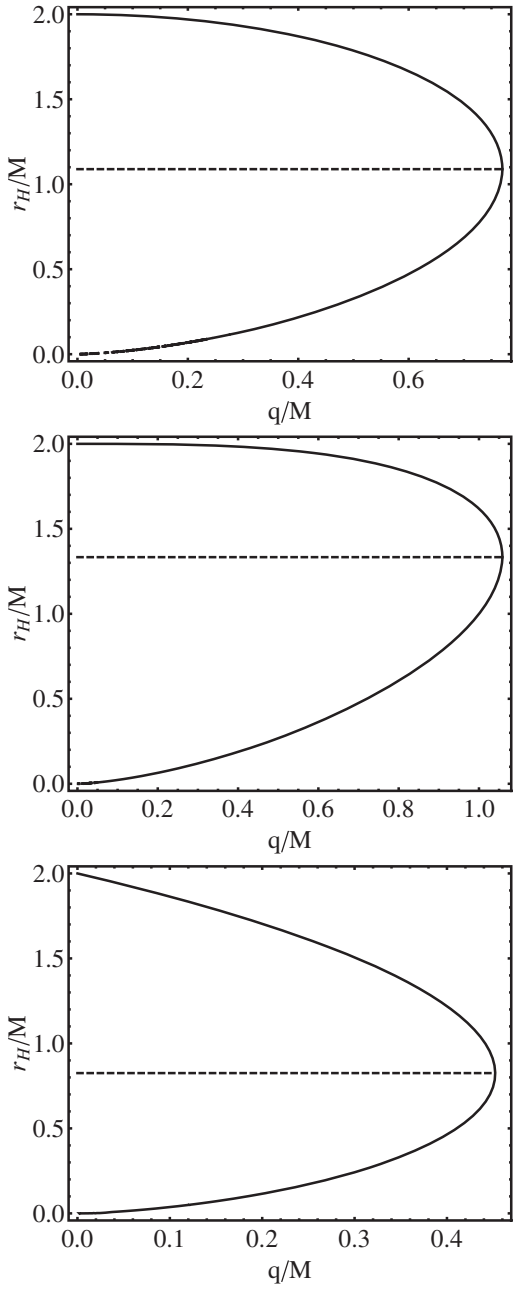

FIG. 2. Inner and outer normalized horizons radii r_H/M versus q/M. The dashed black line marks the border between inner and outer horizons. Top: Bardeen BH with the border $r_H/M = (4\sqrt{2/3})/3 \approx 1.08866$ at $q/M = 4/(3\sqrt{3}) \approx 0.7698$. Middle: Hayward BH with the border $r_H/M = 4/3 \approx 1.33333$ at $q/M = 2^{5/3}/3 \approx 1.058267$. Bottom: Dymnikova BH with the border $r_H/M = 0.82532$ at $q/M = 0.452167$.

successful to model the QPO frequencies also from a statistical viewpoint, see Fig. 1.

For the sake of completeness, it appears that the contour plots obtained from RBHs are sometimes badly shaped. This is particularly evident for the Dymnikova, metric, which appears unsuitable to model QPOs. In view of the above, we conclude that singular spacetime, as a Schwarzschild metric, seem less predictive to frame out the exteriors of a NS, and so finding out new regular spacetimes, *ad hoc* constructed to mode such sources, could represent a future key perspective. In other words, we may speculate that new RBH solutions can better adapt to these kind of problems as we will investigate in incoming efforts.

It is also valuable to investigate and make comparisons between the regular solutions and the singular Kerr spacetime in order to gain further insights. The relativistic precession model has been applied to the BH binary XTE J1550-564, in order to infer both mass and spin of the BH from QPO data points [68]. There, the Kerr metric has been naturally involved to describe the surrounding spacetime around a rotating BH. However, for a NS the underlying geometry is different from the Kerr spacetime. It is even more complicated, as due to spin inducing multipole moments such as mass quadrupole, octupole etc. [100–106]. In the static limit, the geometry around both BHs and NSs can be described by the Schwarzschild or regular solutions. We expect that the inclusion of the spin of a NS will change our outcomes similarly to what happens for QPO data from BH binary systems. Accordingly, to rely on the simplest assumptions possible and to better focus on constraining the smearing parameters of our regular solutions, we neglected the spin of NSs and focus on static configurations. Incoming works will refine our findings adding further information as we will discuss in the conclusions of this work.

Last but not least, following Ref. [47], we see that, among all singular metrics, the de Sitter and/or anti–de Sitter solutions appear to work better in featuring the fits for our sources compared with the Schwarzschild metric. As it is well-known, the de Sitter and anti–de Sitter solutions prompt a cosmological constant term, $\sim\Lambda r^2$, filling the whole spacetime (not only at the center, as in the Hayward picture). The latter term, then, is clearly regular, supporting more our conclusions that seem to favor RBHs.

VI. CONCLUSIONS AND PERSPECTIVES

We here focused on eight NS sources, fitting the corresponding observed frequency data with four QPO models, within the framework of the relativistic precession model. In this respect, we considered three RBH solutions, involving spherical symmetry: Bardeen, Hayward and Dymnikova spacetimes. In addition to these three, for comparison, we considered also the standard Schwarzschild solution. In so doing, we analyzed the aforementioned RBH solutions by means of MCMC fitting procedure based on the Metropolis-Hastings algorithm. Then, our findings have been compared and contrasted by adopting AIC and BIC statistical criteria. Consequently, for each QPO dataset, we computed best fit values, in particular the masses, and inferred the ISCO values for each solution. Our results certify that RBHs can describe NS exteriors and in most of the cases appear to be

better suited than the standard spherical symmetry induced by the Schwarzschild spacetime. To this end, we conclude that among all the RBH involved solutions, the best options remain Bardeen and Hayward spacetimes, whereas the Dymnikova metric is ruled out.

Our results seems to align with those obtained recently in the literature, where two opposite regimes seem to coexist. In fact, for those QPO data that admit RBHs solutions as best-fits, the regularization (or, analogously, the quantum deformation) parameter q is always comparable with the Schwarzschild radius (see Table I), in analogy with recent results [61]. This somehow tells us that in QPO datasets quantum effects seem to be relevant. On the contrary, sources where the effect of the regularization parameter is irrelevant do exist, like in the cases of GX 5–1 ad GX $340+0$ in which q is consistent with a vanishing value, in agreement with other results in the literature [64].

Back to the QPO sources best-described by the Bardeen and the Hayward regular solutions, it is worth noticing that such RBHs require topological charges and/or effective cosmological constant behavior at the center that seem to be relevant to characterize the external of a compact object. Our results, in view of recent findings, suggested that a possible de Sitter and anti–de Sitter core-solutions better fit our sources [47] and the possibility of extending with non-singular metrics remains fully-valid. As direct drawback, we can stress the need of more and better QPO datasets to improve the overall quality of the fits. However, we are convinced that our findings will be compatible with actual results, confirming the Bardeen and Hayward spacetimes.

Future efforts will focus also on studying more RBH solutions that exhibit physical properties different from topological charges. The same procedure can be carried forward involving alternative theories of gravity where RBHs can be investigated, checking whether changing the background is compatible with NS sources. Finally, we will investigate the effects of reconstructed non-singular metrics, i.e., regular solutions inferred directly from data, instead of postulating a given one from the very beginning, adopting some sort of *back-scattering procedure* of reconstruction. Moreover, we may also follow the general procedure for constructing exact BH solutions with electric or magnetic charges, as proposed in Ref. [107] and utilized in Ref. [62] to model the S2 data. In addition, we will test the RBHs with frameworks different from the relativistic precession model.

ACKNOWLEDGMENTS

O. L. is grateful to the Department of Physics of the Al-Farabi University for hospitality during the period in which this manuscript has been written. O. L. acknowledges Roberto Giambò for fruitful discussions on the subject of this paper. K. B. acknowledges Mariano Mendez for providing QPO data. This research has been partially funded by the Science Committee of the Ministry of Science and Higher Education of the Republic of Kazakhstan (Grant No. AP19680128).

APPENDIX: CONTOUR PLOTS OF THE REGULAR SPACETIMES

Figures 3–5 display the contour plots of the RBH solutions considered in this work. The best-fit model parameters of these contours can be obtained by looking at the results of Table I and considering the definitions in Secs. III A–III C of the parameter q in terms of the model parameters of each regular solution.

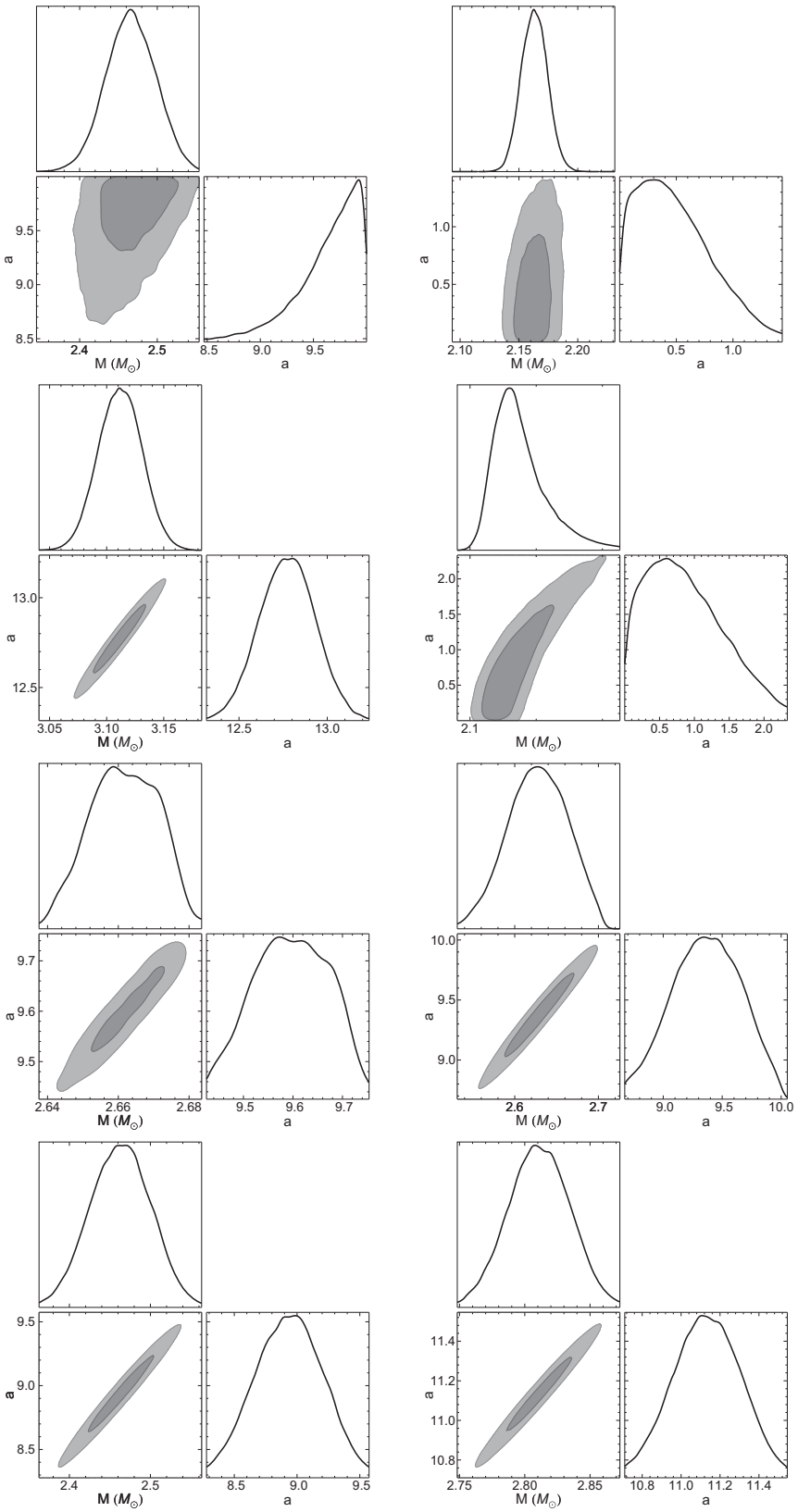

FIG. 3. The Hayward metric contours plots of the best-fit parameters (black dots) and the associated 1–σ (dark gray) and 2–σ (light gray) confidence regions of the sources listed in Table I. Top panels, from left to right: Cir X1, GX 5-1, GX 17 + 2, and GX 340 + 0. Bottom line, from left to right: Sco X1, 4U1608-52, 4U1728-34, and 4U0614 + 091.

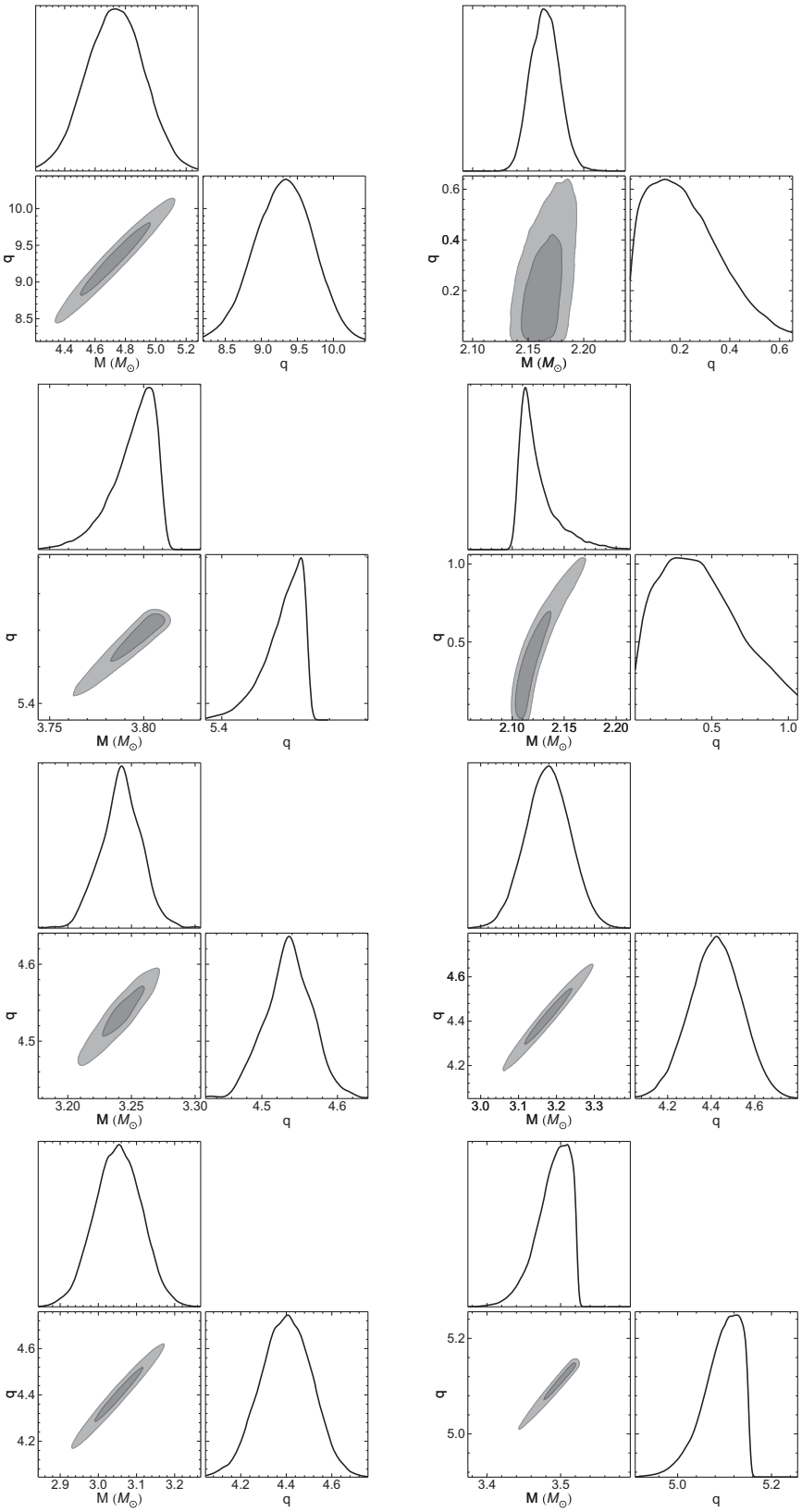

FIG. 4. The same as in Fig. 3 but for the Bardeen metric.

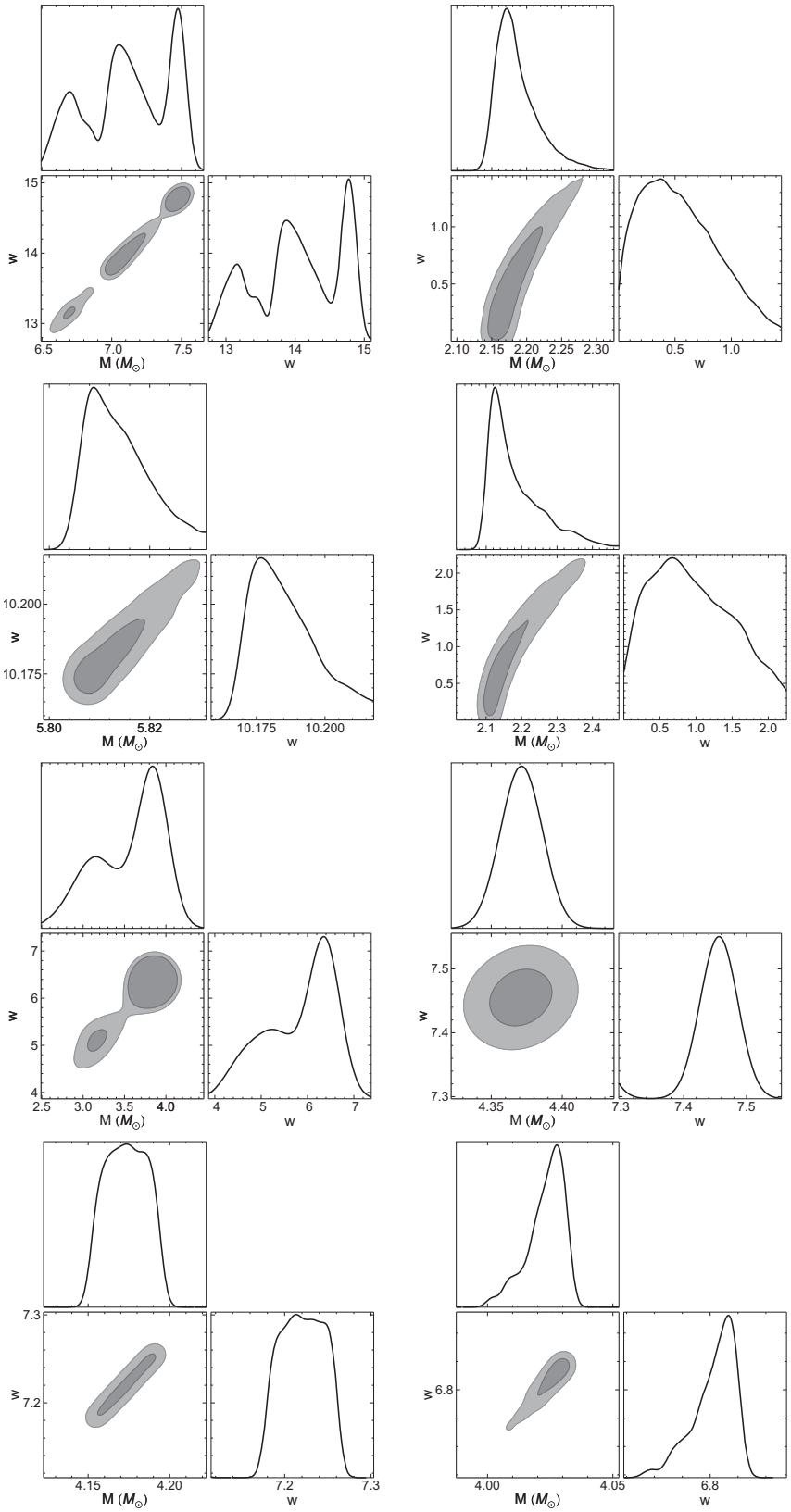

FIG. 5. The same as in Fig. 3 but for Dymnikova metric.

[1] B. P. Abbott, R. Abbott, T. D. Abbott, M. R. Abernathy, F. Acernese, K. Ackley, C. Adams, T. Adams, P. Addesso, R. X. Adhikari *et al.*, Phys. Rev. Lett. **116**, 061102 (2016).

[2] K. Akiyama, A. Alberdi, W. Alef, K. Asada, R. Azulay, A.-K. Baczko, D. Ball, M. Baloković, J. Barrett *et al.* (Event Horizon Telescope Collaboration), Astrophys. J. Lett. **875**, L1 (2019).

[3] A. V. Astashenok, S. Capozziello, and S. D. Odintsov, J. Cosmol. Astropart. Phys. 01 (2015) 001.

[4] A. V. Astashenok, S. Capozziello, and S. D. Odintsov, J. Cosmol. Astropart. Phys. 12 (2013) 040.

[5] A. V. Astashenok, S. D. Odintsov, and A. de la Cruz-Dombriz, Classical Quantum Gravity **34**, 205008 (2017).

[6] S. Capozziello, R. D'Agostino, and O. Luongo, Int. J. Mod. Phys. D **28**, 1930016 (2019).

[7] A. V. Astashenok, S. Capozziello, S. D. Odintsov, and V. K. Oikonomou, Phys. Lett. B **811**, 135910 (2020).

[8] M. Volonteri, M. Habouzit, and M. Colpi, Nat. Rev. Phys. **3**, 732 (2021).

[9] H. V. D. Bradt and J. E. McClintock, Annu. Rev. Astron. Astrophys. **21**, 13 (1983).

[10] J. Wang, Int. J. Astron. Astrophys. **6**, 82 (2016).

[11] J. van Paradijs and J. E. McClintock, in *X-ray Binaries* (Cambridge Astrophysics, Cambdrige, 1995), pp. 58–125.

[12] M. van der Klis, in *Compact Stellar X-Ray Sources* (Cambridge University Press, Cambridge, England, 2006), Vol. 39, pp. 39–112.

[13] F. K. Lamb and S. Boutloukos, *Accreting Neutron Stars in Low-Mass X-Ray Binary Systems* (Springer Netherlands, Dordrecht, 2008), pp. 87–109, ISBN: 978-1-4020-6544-6.

[14] L. Stella and M. Vietri, Nucl. Phys. B, Proc. Suppl. **69**, 135 (1999).

[15] K. Boshkayev, D. Bini, J. Rueda, A. Geralico, M. Muccino, and I. Siutsou, Gravitation Cosmol. **20**, 233 (2014).

[16] K. Boshkayev, J. Rueda, and M. Muccino, Astronomy Reports **59**, 441 (2015).

[17] G. Török, K. Goluchová, M. Urbanec, E. Šrámková, K. Adámek, G. Urbancová, T. Pecháček, P. Bakala, Z. Stuchlík, J. Horák *et al.*, Astrophys. J. **833**, 273 (2016).

[18] K. Boshkayev, J. A. Rueda, and M. Muccino, in *Fourteenth Marcel Grossmann Meeting—MG14*, edited by M. Bianchi, R. T. Jansen, and R. Ruffini (World Scientific, 2018), pp. 3433–3440.

[19] J. Middleditch, Astrophys. J. Lett. **257**, L71 (1982).

[20] S. Larsson, Astron. Astrophys. **181**, L15 (1987).

[21] S. Larsson, Astron. Astrophys. **217**, 146 (1989).

[22] J. M. Bonnet-Bidaud, M. Mouchet, C. Busschaert, E. Falize, and C. Michaut, Astron. Astrophys. **579**, A24 (2015).

[23] M. van der Klis, F. Jansen, J. van Paradijs, W. H. G. Lewin, E. P. J. van den Heuvel, J. E. Trumper, and M. Szatjno, Nature (London) **316**, 225 (1985).

[24] J. Middleditch and W. C. Priedhorsky, Astrophys. J. **306**, 230 (1986).

[25] W. Kluźniak, J. P. Lasota, M. A. Abramowicz, and B. Warner, Astron. Astrophys. **440**, L25 (2005).

[26] C. M. Zhang, H. X. Yin, and Y. H. Zhao, Publ. Astron. Soc. Pac. **119**, 393 (2007).

[27] T. M. Belloni, A. Sanna, and M. Méndez, Mon. Not. R. Astron. Soc. **426**, 1701 (2012).

[28] C. Bambi, D. Malafarina, and N. Tsukamoto, Phys. Rev. D **89**, 127302 (2014).

[29] C. Bambi, A. D. Dolgov, and A. A. Petrov, J. Cosmol. Astropart. Phys. 09 (2009) 013.

[30] J. E. McClintock, R. Narayan, S. W. Davis, L. Gou, A. Kulkarni, J. A. Orosz, R. F. Penna, R. A. Remillard, and J. F. Steiner, Classical Quantum Gravity **28**, 114009 (2011).

[31] M. Kološ, M. Shahzadi, and Z. Stuchlík, Eur. Phys. J. C **80**, 133 (2020).

[32] M. C. Miller, F. K. Lamb, and D. Psaltis, Astrophys. J. **508**, 791 (1998).

[33] L. Titarchuk, I. Lapidus, and A. Muslimov, Astrophys. J. **499**, 315 (1998).

[34] F. K. Lamb and M. C. Miller, Astrophys. J. **554**, 1210 (2001).

[35] P. C. Fragile, G. J. Mathews, and J. R. Wilson, Astrophys. J. **553**, 955 (2001).

[36] M. A. Abramowicz and W. Kluźniak, Astron. Astrophys. **374**, L19 (2001).

[37] L. Titarchuk and K. Wood, Astrophys. J. Lett. **577**, L23 (2002).

[38] P. Rebusco, Publ. Astron. Soc. Jpn. **56**, 553 (2004).

[39] S. Kato, Publ. Astron. Soc. Jpn. **57**, L17 (2005).

[40] S. Kato, Publ. Astron. Soc. Jpn. **64**, 139 (2012).

[41] I. Banerjee, J. Cosmol. Astropart. Phys. 05 (2022) 020.

[42] L. Stella and M. Vietri, Astrophys. J. Lett. **492**, L59 (1998).

[43] L. Stella and M. Vietri, Phys. Rev. Lett. **82**, 17 (1999).

[44] L. Stella, M. Vietri, and S. M. Morsink, Astrophys. J. Lett. **524**, L63 (1999).

[45] S. E. Motta, T. Belloni, L. Stella, G. Pappas, J. Casares, A. T. Muñoz-Darias, M. A. P. Torres, and I. V. Yanes-Rizo, Mon. Not. R. Astron. Soc. **517**, 1469 (2022).

[46] K. Rink, I. Caiazzo, and J. Heyl, Mon. Not. R. Astron. Soc. **517**, 1389 (2022).

[47] K. Boshkayev, O. Luongo, and M. Muccino, arXiv:2212.10186.

[48] C. B. Singh, S. Mondal, and D. Garofalo, Mon. Not. R. Astron. Soc. **510**, 807 (2022).

[49] C. Bellavita, F. García, M. Méndez, and K. Karpouzas, Mon. Not. R. Astron. Soc. **515**, 2099 (2022).

[50] Z. Stuchlík, M. Kološ, and A. Tursunov, Publ. Astron. Soc. Jpn. **74**, 1220 (2022).

[51] Y. Zhang, M. Méndez, F. García, K. Karpouzas, L. Zhang, H. Liu, T. M. Belloni, and D. Altamirano, Mon. Not. R. Astron. Soc. **514**, 2891 (2022).

[52] A. R. Ingram and S. E. Motta, Nature (London) **85**, 101524 (2019).

[53] S. E. Motta, Astron. Nachr. **337**, 398 (2016).

[54] R. Penrose, Phys. Rev. Lett. **14**, 57 (1965).

[55] S. W. Hawking and R. Penrose, Proc. R. Soc. A **314**, 529 (1970).

[56] J. M. Bardeen, *Proceedings of the International Conference GR5* Tbilisi, U.S.S.R. (1968).

[57] E. Ayón-Beato and A. García, Phys. Lett. B **493**, 149 (2000).

[58] E. Ayón-Beato and A. García, Phys. Rev. Lett. **80**, 5056 (1998).
[59] I. Dymnikova, Gen. Relativ. Gravit. **24**, 235 (1992).
[60] S. A. Hayward, Phys. Rev. Lett. **96**, 031103 (2006).
[61] M. Cadoni, M. Oi, and A. P. Sanna, Phys. Rev. D **106**, 024030 (2022).
[62] M. Cadoni, M. De Laurentis, I. De Martino, R. Della Monica, M. Oi, and A. P. Sanna, Phys. Rev. D **107**, 044038 (2023).
[63] J. Mazza, E. Franzin, and S. Liberati, J. Cosmol. Astropart. Phys. 04 (2021) 082.
[64] S. Riaz, S. Shashank, R. Roy, A. B. Abdikamalov, D. Ayzenberg, C. Bambi, Z. Zhang, and M. Zhou, J. Cosmol. Astropart. Phys. 10 (2022) 040.
[65] S. Guo, G.-R. Li, and E.-W. Liang, Phys. Rev. D **105**, 023024 (2022).
[66] F. Lamy, E. Gourgoulhon, T. Paumard, and F. H. Vincent, Classical Quantum Gravity **35**, 115009 (2018).
[67] C. Bambi and S. Nampalliwar, Europhys. Lett. **116**, 30006 (2016).
[68] S. E. Motta, T. Munoz-Darias, A. Sanna, R. Fender, T. Belloni, and L. Stella, Mon. Not. R. Astron. Soc. **439**, L65 (2014).
[69] S. E. Motta, T. M. Belloni, L. Stella, T. Muñoz-Darias, and R. Fender, Mon. Not. R. Astron. Soc. **437**, 2554 (2014).
[70] T. Muller and F. Grave, arXiv:0904.4184.
[71] C. Bambi and L. Modesto, Phys. Lett. B **721**, 329 (2013).
[72] A. Kamenshchik and P. Petriakova, Phys. Rev. D **107**, 124020 (2023).
[73] P. Beltracchi and P. Gondolo, Phys. Rev. D **104**, 124066 (2021).
[74] U. Kumar, S. Panda, and A. Patel, Eur. Phys. J. C **80**, 614 (2020).
[75] H. C. D. L. Junior, L. C. B. Crispino, P. V. P. Cunha, and C. A. R. Herdeiro, Eur. Phys. J. C **80**, 1036 (2020).
[76] X. Ye, C.-H. Wang, and S.-W. Wei, arXiv:2306.12097.
[77] M. S. Volkov, Phys. Rev. D **104**, 124064 (2021).
[78] A. C. Gutiérrez-Piñeres, N. H. Beltrán, and C. S. López-Monsalvo, J. Phys. Conf. Ser. **2081**, 012005 (2021).
[79] D. Hansen and N. Yunes, Phys. Rev. D **88**, 104020 (2013).
[80] A. C. Gutiérrez-Piñeres and H. Quevedo, Gen. Relativ. Gravit. **48**, 146 (2016).
[81] E. Poisson and W. Israel, Classical Quantum Gravity **5**, L201 (1988).
[82] P. Dutta Roy and S. Kar, Phys. Rev. D **106**, 044028 (2022).
[83] I. Dymnikova, Classical Quantum Gravity **21**, 4417 (2004).
[84] R. Arjona, W. Cardona, and S. Nesseris, Phys. Rev. D **99**, 043516 (2019).
[85] A. R. Liddle, Mon. Not. R. Astron. Soc. **377**, L74 (2007).
[86] H. T. Cromartie, E. Fonseca, S. M. Ransom, P. B. Demorest, Z. Arzoumanian, H. Blumer, P. R. Brook, M. E. DeCesar, T. Dolch, J. A. Ellis *et al.*, Nat. Astron. **4**, 72 (2020).
[87] S. Boutloukos, M. van der Klis, D. Altamirano, M. Klein-Wolt, R. Wijnands, P. G. Jonker, and R. P. Fender, Astrophys. J. **653**, 1435 (2006).
[88] G. Török, P. Bakala, E. Šrámková, Z. Stuchlík, and M. Urbanec, Astrophys. J. **714**, 748 (2010).
[89] R. Wijnands, M. Méndez, M. van der Klis, D. Psaltis, E. Kuulkers, and F. K. Lamb, Astrophys. J. Lett. **504**, L35 (1998).
[90] P. G. Jonker, M. van der Klis, J. Homan, M. Méndez, W. H. G. Lewin, R. Wijnands, and W. Zhang, Mon. Not. R. Astron. Soc. **333**, 665 (2002).
[91] J. Homan, M. van der Klis, P. G. Jonker, R. Wijnands, E. Kuulkers, M. Méndez, and W. H. G. Lewin, Astrophys. J. **568**, 878 (2002).
[92] P. G. Jonker, M. van der Klis, R. Wijnands, J. Homan, J. van Paradijs, M. Méndez, E. C. Ford, E. Kuulkers, and F. K. Lamb, Astrophys. J. **537**, 374 (2000).
[93] F. Cipolletta, C. Cherubini, S. Filippi, J. A. Rueda, and R. Ruffini, Phys. Rev. D **92**, 023007 (2015).
[94] M. Méndez and M. van der Klis, Mon. Not. R. Astron. Soc. **318**, 938 (2000).
[95] R. Belvedere, K. Boshkayev, J. A. Rueda, and R. Ruffini, Nucl. Phys. **A921**, 33 (2014).
[96] A. M. Cherepashchuk, T. S. Khruzina, and A. I. Bogomazov, Mon. Not. R. Astron. Soc. **508**, 1389 (2021).
[97] M. Méndez, M. van der Klis, R. Wijnands, E. C. Ford, J. van Paradijs, and B. A. Vaughan, Astrophys. J. Lett. **505**, L23 (1998).
[98] M. Méndez and M. van der Klis, Astrophys. J. Lett. **517**, L51 (1999).
[99] E. C. Ford, P. Kaaret, K. Chen, M. Tavani, D. Barret, P. Bloser, J. Grindlay, B. A. Harmon, W. S. Paciesas, and S. N. Zhang, Astrophys. J. Lett. **486**, L47 (1997).
[100] J. B. Hartle, Astrophys. J. **150**, 1005 (1967).
[101] J. B. Hartle and K. S. Thorne, Astrophys. J. **153**, 807 (1968).
[102] H. Quevedo and B. Mashhoon, Phys. Lett. **109A**, 13 (1985).
[103] W. G. Laarakkers and E. Poisson, Astrophys. J. **512**, 282 (1999).
[104] V. S. Manko, E. W. Mielke, and J. D. Sanabria-Gómez, Phys. Rev. D **61**, 081501 (2000).
[105] L. A. Pachón, J. A. Rueda, and J. D. Sanabria-Gómez, Phys. Rev. D **73**, 104038 (2006).
[106] G. Pappas, Mon. Not. R. Astron. Soc. **422**, 2581 (2012).
[107] Z.-Y. Fan and X. Wang, Phys. Rev. D **94**, 124027 (2016).